# Sources of Motion-Sensitivity Loss in Glaucoma

*Helle K. Falkenberg*[1] *and Peter J. Bex*[2]

**Purpose.** Primary open angle glaucoma (POAG) is a leading cause of irreversible adult blindness and is characterized by progressive optic neuropathy and constriction of the visual field. Behavioral tests for POAG target retinal ganglion cell (RGC) classes that have reduced redundancy or that might be selectively damaged, but these tests cannot differentiate dysfunctional from nonfunctional RGC inputs to motion sensors. In this study, a signal-to-noise motion-sensitivity task was used to investigate the sources of motion-sensitivity loss in patients with POAG.

**Methods.** An equivalent noise paradigm was used to investigate sensitivity to the direction of radial optic flow patterns across the visual field in visually normal observers and patients with POAG. Internal noise and sampling efficiency were estimated from the direction of heading contrast-discrimination thresholds as a function of the level of added external noise.

**Results.** Contrast sensitivity to optic flow fell with retinal eccentricity for all observers, and decreased with both age and POAG. Equivalent noise analysis showed that the fall-off with eccentricity was primarily due to reduced sampling efficiency with relatively little increase in the level of internal noise and that the fall-off with age was attributable to both sources of error. Compared with age-matched control observers, patients with POAG have similar levels of internal noise but significantly lower sampling efficiency at all retinal loci.

**Conclusions.** Motion-sensitivity losses with age, eccentricity, and POAG can arise from higher levels of internal noise and lower sampling efficiency. The central and peripheral glaucomatous neuropathy is mostly attributable to a reduction in sampling efficiency, suggesting that RGCs are nonfunctional rather than dysfunctional in this condition. (*Invest Ophthalmol Vis Sci.* 2007;48:2913–2921) DOI:10.1167/iovs.06-0752

Primary open-angle glaucoma (POAG) is a blinding disease that is characterized by progressive optic neuropathy and loss of the visual field caused by progressive dysfunction or death of retinal ganglion cells (RGCs). POAG is a leading cause of irreversible visual impairment in the developed world[1,2] and the second major cause of blindness globally.[3] It has a prevalence of 1.5% to 8.5% in people over the age of 40 years, depending on the study method and ethnic group examined.[4–9] POAG is an age-related eye disease, and the growing elderly population means that the morbidity associated with this condition will rise.[10,11] Postmortem studies show a loss of RGCs in glaucomatous eyes, but the pathophysiology of the progressive degeneration of RGCs is still poorly understood. The site of damage is commonly accepted to be the nerve fibers at the level of the lamina cribrosa,[12,13] but the mechanisms of damage, whether by necrosis, apoptosis, or another mechanism,[12] is still mainly unknown (for review, see Ref. 14). More recently, there has been evidence that POAG causes neural degeneration in the human lateral geniculate nucleus and visual cortex.[13] Because POAG is treatable and because the visual loss from the disease is irreversible, early detection is vital.[14]

Early POAG is asymptomatic, and diagnosis is based on examination of the optic nerve head, retinal nerve fiber layer, visual fields, and intraocular pressure. Visual fields have been tested traditionally with white-on-white perimetry (for review, see Refs. 15–17), which, although clinically useful, is relatively insensitive to early RGC dysfunction.[18–20] Histologic cell counts show that as many as 60% of RGCs may be lost before a visual defect can be detected by conventional perimetry[18,21–23] (although the underlying trends may show a linear fall-off in sensitivity[24]) and that there is a poor relationship between conventional perimetry and optic disc change.[25,26] These concerns have lead to a search for more sensitive behavioral measures for the early detection of POAG.

To this end, many groups have tried to detect visual sensitivity deficits for moving and flickering[27–37] or short-wavelength[28,38–42] stimuli, because these stimuli are detected by pathways involving RGC classes that may be selectively damaged in POAG.[17,26,28] The motion-sensitivity deficit is thought to depend on selective impairment of magnocellular RGCs, which, among other RGC classes, are sensitive to moving images[43,44] and have large cell bodies and axons that may be vulnerable to glaucomatous damage.[45] Perhaps more important, both magnocellular and short-wavelength sensitive pathways are less redundant,[42] owing to the relatively sparse distribution of magnocellular (5%–10%) and bistratified (1%–7%) RGCs. However, studies directly comparing glaucomatous sensitivity loss for motion perimetry and conventional perimetry have not always found a selective loss for moving stimuli,[37,46–49] and other studies have found no significant differences in sensitivity loss for stimuli of low spatial and high temporal frequency.[50,51] This problem could be the consequence of the significant overlap in the response selectivity of mango- and parvo RGCs.[46,52]

Motion- and short-wavelength perimetry can detect sensitivity losses in glaucoma, but they are unable to determine whether the problem is caused by increased levels of internal noise or by a reduction in sampling efficiency. It is also unclear whether changes in noise or sampling efficiency account for motion-sensitivity changes with eccentricity and in the normal aging process.[53–59] We adapted an equivalent noise (EN) paradigm to separate these two sources of sensory impairment in POAG by using natural optic flow movies, as illustrated in Figure 1. The perception of optic flow is important for self-motion, estimating time until collision with other objects or persons, and safe navigation in our environment, and it is well documented that patients with peripheral visual field loss show impaired mobility performance.[60–62] In addition we used the EN paradigm to investigate the sensitivity to these complex optic flow stimuli across the retina and in normal ageing in control observers. We further developed a model of global motion detection that mimics the effects of increased RGC

From the [1]Department of Optometry and Vision Science, Buskerud University College, Kongsberg, Norway; and the [2]The Schepens Eye Research Institute, Harvard Medical School, Boston, Massachusetts.

Supported by The Wellcome Trust.

Submitted for publication July 4, 2006; revised October 19, 2006; accepted April 10, 2007.

Disclosure: **H.K. Falkenberg**, None; **P.J. Bex**, None

The publication costs of this article were defrayed in part by page charge payment. This article must therefore be marked "*advertisement*" in accordance with 18 U.S.C. §1734 solely to indicate this fact.

Corresponding author: Helle K. Falkenberg, Department of Optometry and Vision Science, Buskerud University College, Frogsvei 41, Kongsberg, Norway; helle.falkenberg@hibu.no.

internal noise and reduced RGC sampling efficiency. When the local motion inputs to the model are lesioned to simulate RGC loss, the model accurately reproduces the observer's behavior.

## METHODS

### Observers

Nineteen observers participated in the study: four young observers (mean age, 30.5 ±6.4 years) and eight healthy, age-matched control (AMC) observers (mean age, 74.2 ± 5.1 years), with full visual fields, and seven patients with POAG (mean age, 72.3 ± 7.4 years). Patients with POAG were recruited from the glaucoma clinic at Moorfields Eye Hospital. All patients had peripheral visual field loss (mean AGIS score, 8.4 ± 5.2[63]) outside the central 12° as determined by Humphrey 24-2 perimetry (HFA; Carl Zeiss Meditec, Welwyn Garden City, UK). Informed consent was obtained from each observer and ethical approval was obtained from participating institutions. The protocol conformed to the tenets of the Declaration of Helsinki. Observers were excluded from the study if they had refractive errors greater than 5 D equivalent sphere, visual acuity worse than 0.48 logMAR (6/18), or any coexisting medical conditions.

### Stimuli and Procedure

Real-scene linear digital movies of the visual field at a constant driving speed of 50 km/h were recorded with a camera (NV-GS200EB; Panasonic, Bracknell, UK)[64] and presented on a monitor (1152 × 864 pixels; Triniton Multiscan G500; Sony, Tokyo, Japan) at a frame rate of 75 Hz and a mean luminance of 50 cd/m$^2$. The luminance of the display was calibrated with a chromometer (CS100; Konica Minolta, Osaka, Japan), and a bit-stealing algorithm was used to obtain 10.8 bits (1785 levels) of luminance resolution.[65] The stimulus was viewed monocularly with appropriate correction for a viewing distance of 57 cm in an otherwise dark room.

Each trial, a 0.64-second section of the movie (16 sequential video frames) was selected from a random starting point using routines from commercial software (MatLab; The MathWorks, Natick, MA) and the Psychophysics toolbox.[66] The RGB (red-green-blue) values of each 320 × 240-pixel source movie frame were averaged to produce a monochrome image that was scaled to a 0 mean. The images were cropped horizontally and zero padded vertically to produce 16 experimental movie frames, each 256 × 256 pixels. A 1/*f* noise-mask movie was generated by randomizing the phase spectrum of the experimental movie in the frequency domain without altering its amplitude spectrum. The zero mean target and mask movies were scaled so that the standard deviation of the pixel values gave the required root mean square (RMS) contrast. The target and mask movies were then linearly summed and presented within a 4° diameter circular window and finally rescaled between 0 and 255 in RGB for presentation on the computer monitor. The edges of the window were smoothed over 0.5° (which obscured the vertical zero-padding) and stimulus onset and offset were smoothed over 50 ms with raised cosine functions. The RMS contrast of the target movie was under the control of a staircase[67] and the RMS contrast of the mask was fixed between 0 and 0.32. The experimental movie frames were presented on alternate video frames of the 75-Hz CRT monitor, so that the stimulus lasted 427 ms in total.

The direction of target motion was randomized from trial to trial by presenting the experimental movie in forward or reverse sequence. The observer's task was to maintain steady fixation and indicate with a button press whether the direction of heading (DOH) was forward (expansion) or backward (contraction). Feedback was provided at the fixation point for incorrect responses. Identical results were obtained with random dot stimuli, but lacked the behavioral relevance of natural scenes. Compliant fixation was monitored with an eye-tracking system (50 Hz, Video Eyetracker Toolbox; Cambridge Research Systems, Cambridge, UK). If fixation strayed beyond 0.75° (24 pixels) from the fixation mark, auditory feedback was provided, and the trial was discarded. Fixation calibration was performed before each run and required the observer to fixate 20 points presented in a random matrix order across the display.

Young and AMC observers performed the task at three eccentricities (fovea and 8° and 16° in the nasal visual field, to avoid the optic disc), whereas patients with POAG performed the experiments at two retinal eccentricities (fovea and 8°), to avoid placing the stimulus within the peripheral scotoma. At each eccentricity, contrast thresholds for DOH identification were measured for at least three levels of mask contrast noise (Fig. 1). The contrast of the test stimulus was under control of a three-down, one-up adaptive staircase[67] that adjusted the RMS contrast to a level that produced 79.4% correct responses. Each staircase terminated after 60 trials or eight reversals, whichever occurred first.

### EN Paradigm

At least two factors could limit the precision with which the DOH can be estimated from radial optic flow stimuli. In principle, DOH detection requires that observers first detect local velocity vectors at multiple locations across the scene, then integrate as many local vectors as possible to maximize efficient integration of the information present in the stimulus. We adopt an EN paradigm, first developed by Barlow[68] and adapted to study the perception of blur,[69] orientation,[70] and motion.[71,72] On the assumption that visual performance is limited by internal noise in the visual system and suboptimal sampling efficiency[73] the EN paradigm exploits the additivity of variance in the stimulus and variance in the visual system, so that thresholds can be expressed as

$$\sigma_{DOH} = \sqrt{\frac{\sigma_i^2 + \sigma_c^2}{n}}, \quad (1)$$

where $\sigma_{DOH}$ is the DOH discrimination threshold, $\sigma_i$ is internal noise in the visual system, $\sigma_c$ is external noise in the stimulus, and $n$ is the sampling efficiency (i.e., the proportion of the stimulus that supports the observer's response). Figure 1D illustrates how discrimination thresholds are influenced by internal noise and sampling efficiency. The standard curve (green) shows how thresholds are expected to increase with external noise for an arbitrary observer. The red curve shows that thresholds increase mostly at low noise levels when internal noise is increased but sampling efficiency remains unchanged. Alternatively, when sampling efficiency is reduced but internal noise remains fixed (blue curve), thresholds increase at all levels, particularly at high levels of external noise. We adapted the EN paradigm for direction of heading perception by measuring the minimum stimulus contrast needed to discriminate the DOH in various levels of external added noise in a two-alternative, forced-choice (2AFC) task. Contrast discrimination thresholds for expanding or contracting real-image flow fields in noise were measured as a function of retinal eccentricity.

### Statistical Analysis

The raw data from a minimum of four repetitions were combined and fit with a cumulative normal function by least $\chi^2$ (in which the data are weighted by the binomial standard deviation, calculated from the observed proportion correct and the number of trials tested at each level). DOH contrast discrimination thresholds were estimated from the 75% correct point of the psychometric function. The 95% confidence intervals on this point were calculated with a bootstrap procedure, based on 1000 data sets simulated from the number of experimental trials at each level tested.[74]

The experimental results were considered in terms of threshold differences between the three observer groups and individual differences within groups. Least-square estimates[75] and repeated-measures analysis of variance (ANOVA) were used to determine the internal noise and sampling efficiency and to examine how each differed between groups.

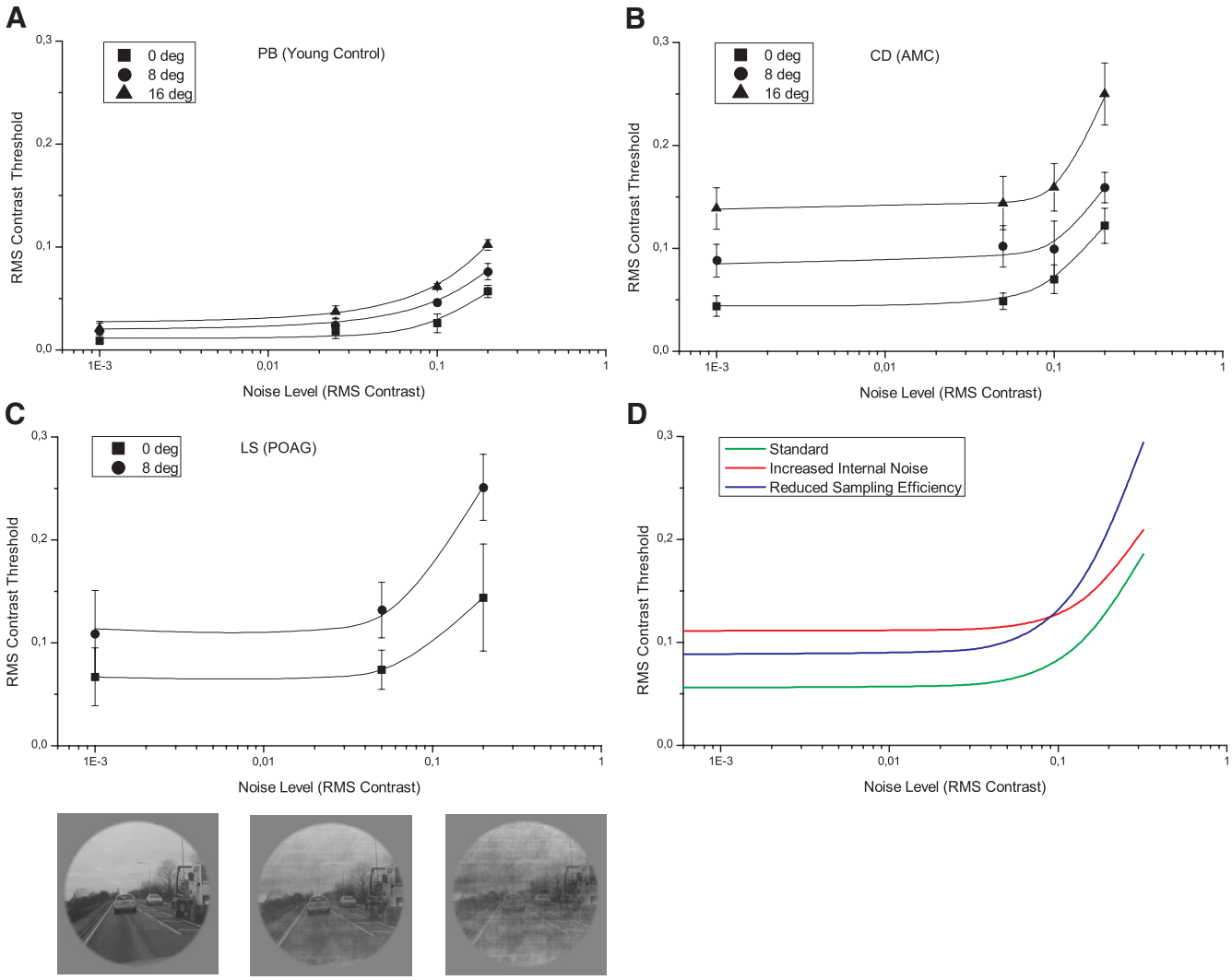


**Figure 1.** Direction discrimination thresholds in noise for normally sighted (**A**) younger and (**B**) older AMC observers and (**C**) a patient with POAG. Data show the RMS contrast of a driving movie required to detect the direction of heading (forwards or backwards) in dynamic noise of fixed RMS contrast (*x*-axis) at an eccentricity indicated by the legend. Error bars, 95% CI. Curves show the fits (least squares, weighted by the confidence intervals) of an EN model illustrated in (**D**) in which internal noise and sampling efficiency were free parameters. (**D**) EN analysis for an arbitrary observer. The standard curve (*green*) shows how thresholds increased with external noise. The *red* curve shows that thresholds increased mostly at low noise levels when internal noise was increased but sampling efficiency remained unchanged. Alternatively, when sampling efficiency is reduced but internal noise remains fixed (*blue curve*), thresholds increase at all levels, particularly at high levels of external noise.

## Results

Figures 1A–C show contrast thresholds for DOH identification as a function of external noise contrast in the central (0°) and peripheral (8° and 16°) visual fields in representative (Fig. 1A) young, (Fig. 1B) age-matched control (AMC) observers, or (Fig. 1C) observers with POAG (the data for all 19 observers are available on request). In all observers, thresholds increased with external noise contrast and with eccentricity. It can also be seen that thresholds were lowest in the young observers at all eccentricities. The curves show fits of the EN analysis (equation 1). The estimated internal noise and sampling efficiencies from the EN fits to all observers are shown in Figures 2 and 3, together with the means for each group.

Figure 2 shows the estimated internal noise as a function of eccentricity in the young control subjects, AMC observers, and patients with POAG, as indicated in the headings. The group means are shown in Figure 2A (error bars show 95% confidence intervals). Individual data are shown in Figures 2B–D, and it can be seen that the group mean is a fair representation of the individual data. The fitted lines are linear regression fits estimated by least squares. There was no significant effect of eccentricity ($F_{(3,43)} = 0.15$, $P = 0.69$, repeated measures ANOVA) for either group. However, the internal noise was significantly lower in the young than in the old observers ($F_{(1,45)} = 6.3$, $P = 0.01$), and more important, internal noise levels were not significantly higher in the patients with glaucoma than in the normally sighted AMC observers ($F_{(1,35)} = 1.1$, $P = 0.26$).

Sampling efficiency is plotted as a function of eccentricity in Figure 3. Figure 3A shows the group means and, as indicated in the legend, individual data are plotted in Figures 3B–D. Error bars show 95% confidence intervals. Sampling efficiency is expressed relative to the efficiency of 1000 trials by an ideal observer, which used every pixel on every frame to make a 2AFC response with the same stimuli and task as the human observers. The ideal-observer template was the source movie itself in forward or reverse sequence, and its binary decision

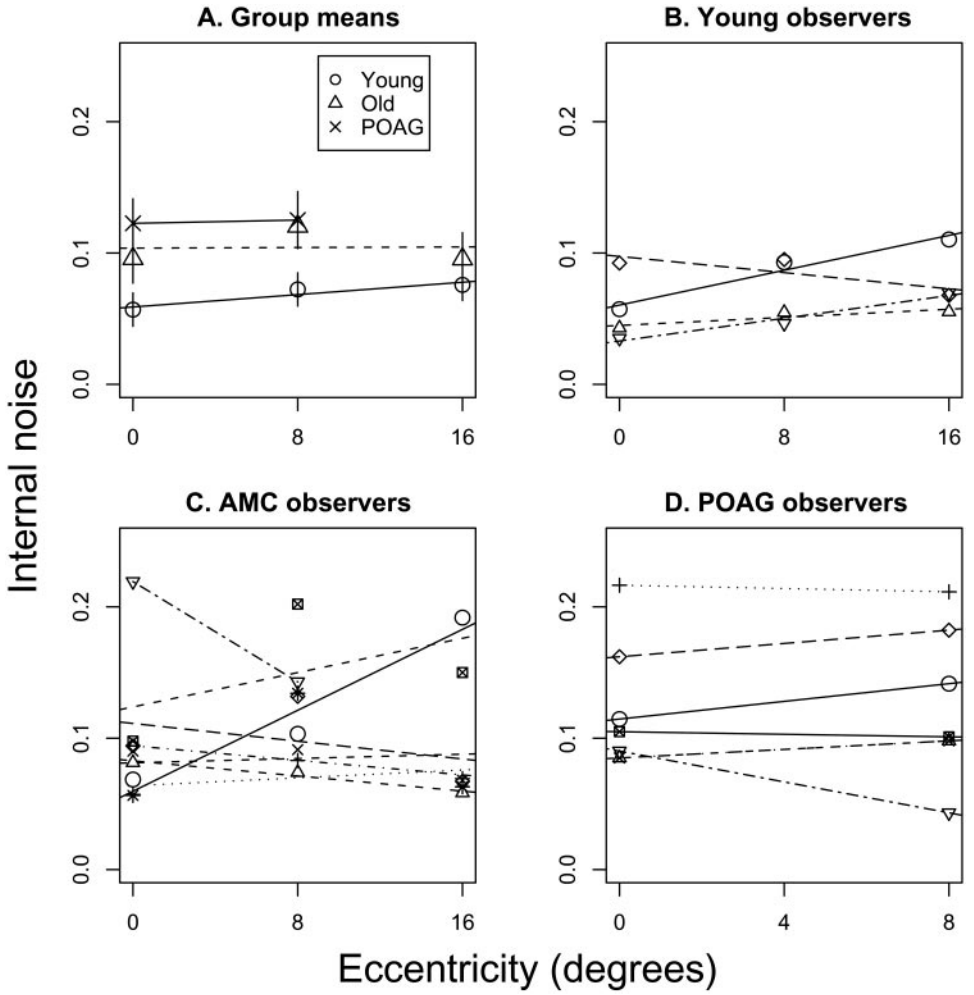


**FIGURE 2.** Internal noise estimates for (**A**) the means of normally sighted (**B**) young and (**C**) AMC observers, and (**D**) patients with POAG. Data show the estimates of internal noise from the EN fits described in Figure 1. In each case, the mean data are representative of the individual subjects. Error bars, 95% confidence limits.

was the sequence producing the highest cross correlation with the stimulus. Relative to the ideal observer, human efficiency can be extremely low, in line with previous studies.[71,76,77]

Again, the group means represent the individual performances fairly. A repeated-measures ANOVA showed that the sampling efficiency was significantly different across groups ($F_{(3,45)} = 38.6$, $P < 0.001$) and was lower in the older observers than in the younger ones ($F_{(1,40)} = 29.1$, $P < 0.001$). There was also a significant reduction in sampling efficiency with eccentricity in the young and AMC observers (young: $F_{(1,10)} = 23.1$, $P < 0.001$; AMC: $F_{(1,21)} = 20.5$, $P < 0.001$). In the patients with glaucoma, sampling efficiency was significantly worse than that in the young or AMC observers ($F_{(1,40)} = 3.7$, $P < 0.001$), but there was no significant change with eccentricity ($F_{(1,12)} = 0.96$, $P = 0.34$).

We developed a model of complex motion processing to simulate the effects of increased internal noise or reduced sampling efficiency (Fig. 4). The movie sequence (eight sequential movies frames, each with 256 × 256 pixels, single frames from which are shown in Fig. 1C) was convolved with a set of eight direction-selective motion energy filters,[78] defined as

$$F_\theta = \frac{1}{\sqrt{2\pi}\sigma_x\sigma_y\sigma_t}\exp\left[-\frac{x^2}{2\sigma_x^2}-\frac{y^2}{2\sigma_y^2}-\frac{t^2}{2\sigma_t^2}+i(\omega_s s_\theta+\omega_t t)\right], \quad (2)$$

where spatial frequency ($\omega_s$) was 16 pixels (equivalent to 2 cyc/deg under our experimental conditions), $s_\theta = x\cos\theta + y\sin\theta$ and the standard deviations of the spatiotemporal Gaussian envelope were $\sigma_x = \sigma_y = 8$ pixels and $\sigma_t = 2$ frames. Single frames of the motion detectors are shown in Figure 4A, with arrows to indicate direction of motion. The response magnitudes for each direction filter were summed across all frames and were used to compute the interpolated direction at each point in the movie:

$$\hat{\theta} = a\tan 2(\textstyle\sum r_\theta(\sin\theta), \sum r_\theta(\cos\theta)), \quad (3)$$

where $\hat{\theta}$ is the interpolated direction and, $r_\theta$ is the response of each filter with peak direction sensitivity at $\theta$.

Figure 4C shows a colored direction map (according to the key shown in 4B) for a typical movie sequence. A binary decision (forward or backward) was based on the greater cross correlation between an expanding (Fig. 4B) or a contracting complex direction template. This binary decision was used for the model to generate contrast direction thresholds in noise, as in the main experiment. Circles and the green curve in Figure 4F show the model behavior as external noise increased. The solid and dashed green curves show the responses of motion filters with a peak spatial frequency of 2 or 4 cyc/deg respectively, which produced almost identical behavior. Noisy RGCs were simulated by adding response noise to the inputs to each motion detector, which produced noisy local direction estimates, as illustrated in Figure 4D. This degraded the model's global motion performance, principally at low noise levels (triangles and red curve in Fig. 4F) and produced higher estimates of internal noise according to EN analysis. RGC loss was simulated by randomly deleting inputs to each motion detector

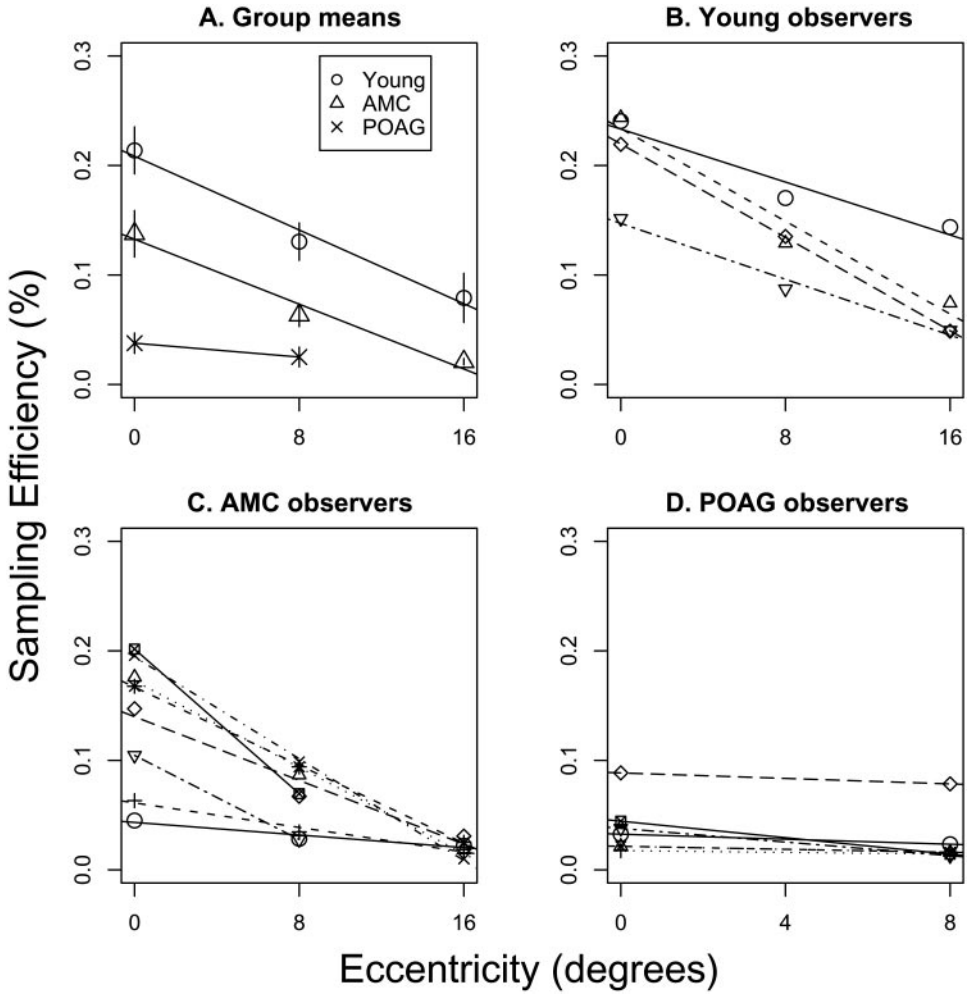


**FIGURE 3.** Sampling efficiency estimates for (**A**) the means of normally sighted (**B**) young and (**C**) AMC observers and (**D**) patients with POAG. Data show the estimates of sampling efficiency from the EN fits described in Figure 1. In each case, the mean data are representative of the individual subjects. Error bars, 95% confidence intervals.

(Fig. 4E). Such lesions degraded model performance principally at high noise levels (squares and blue curve in Figure 4F) and produced lower estimates of sampling efficiency according to EN analysis. This latter pattern of results is similar to that observed in patients with POAG.

## DISCUSSION

In several behavioral studies, it has been found that patients with POAG have reduced motion sensitivity, although it is unclear whether this sensitivity loss is due to increased RGC noise or to reduced RGC sampling efficiency. In this study we showed how an EN paradigm can separate sensitivity loss due to increased internal noise from sensitivity loss due to reduced sampling efficiency (e.g., RGC loss) in a motion-sensitivity task. We examined how these factors change with eccentricity and with age in normally sighted observers and those with POAG. Our results showed that sensitivity to complex motion decreased with age and eccentricity and that there was a further deficit in the patients with POAG compared with the age-matched control observers. This decline in sensitivity was mainly due to a decrease in sampling efficiency, although there was also a small but significant increase in internal noise with age (but not with eccentricity or POAG).

### Motion-Sensitivity Loss in POAG

Our study shows that the patients with POAG had elevated motion contrast discrimination thresholds in response to real optic flow stimuli in central visual field locations that show no deficit on conventional white-on-white perimetry. We found for the first time that this sensitivity loss was due to reduced RGC sampling efficiency and not to increased internal RGC noise. Previous studies have shown that patients with POAG have impaired motion sensitivity,[27–37] but none of these studies has been able to separate these two potential sources of the sensory deficit in living humans. Figures 2A and 3A show how internal noise and sampling efficiency changed with eccentricity in the patients with POAG and in the process of normal aging. It is clear from the data in Figure 2A that there was no evidence of increased levels of internal noise in the patients with POAG compared with that in the age-matched control (AMC) observers, although both these groups showed higher levels of internal noise than did the young observers. However, there was no significant increase in internal noise with eccentricity in the healthy observers or in the patients with POAG.

Figure 3A shows that the patients with POAG had a significantly lower sampling efficiency than did the AMC and young observers, both in the periphery and in the fovea. Previous studies have failed to find global motion-sensitivity loss in the central retina.[34,37] In both of the cited studies, a motion-coherence detection task was used, with high-contrast dot elements. It is possible that high-contrast, random-dot stimuli may not be sensitive enough to detect some motion-sensitivity impairments, because motion coherence performance saturates at very low contrasts.[79] Our paradigm measures the contrast dependence of motion sensitivity parametrically and

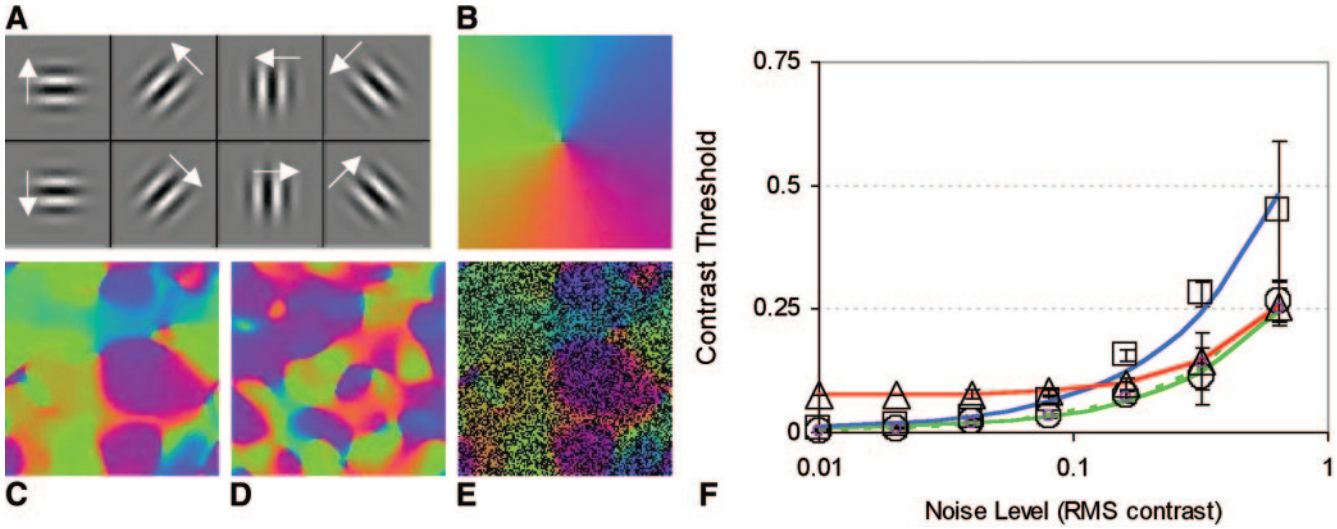


FIGURE 4. Model of complex motion processing and the effects of input noise or lesions. (**A**) Single frames of a bank of motion sensors, with direction selectivity indicated (*arrows*). (**B**) A color-coded direction map of the local direction responses illustrated in (**C–E**), also showing the tuning of the global motion detector for expansion used for the forward–reverse binary decision. (**F**) *Circles* and *green curve*: model behavior as external noise increased. *Solid* and *dashed green curves*: responses of motion filters with a peak spatial frequency of 2 or 4 cyc/deg respectively. *Triangles* and *red curve*: the behavior of the model when dysfunctional RGCs were simulated by adding response noise to the input to each motion sensor. This addition produced noisy local estimates of direction (illustrated in **D**), degraded the model performance principally at low noise levels, and produced higher estimates of internal noise according to the EN analysis. *Squares* and *blue curves*: model simulation to nonfunctional or lost RGCs by randomly deleting inputs to each motion sensor (illustrated schematically in **E**). This deletion degraded the model performance principally at high noise levels and produced lower estimates of sampling efficiency according to EN analysis.

avoids this limitation. It is also possible that the POAG disease process was more advanced in the POAG observers in our study than in the patients in the studies of Joffe et al.[34] (field loss of one point >15 dB, two adjacent points of >10 dB, or three adjacent points of >5 dB) or McKendrick et al.[37] (mean defect [MD] range, −0.99 to −17.45 dB [mean, −8.6]; pattern SD [PSD] range, 2.06–15.11 dB [mean 8.14]). We used an AGIS score[63] (which depends on the number, location, and depth of defect) to quantify the severity of POAG visual field loss. Our patients with POAG had an MD range of −0.88 to −24.29 dB (mean, −9.43) and a PSD range 2.15 to 16.22 dB (mean, 8.64), which is slightly worse than in the other studies. It is therefore possible that the disease had progressed to more foveal areas in the patients in the present study, although none of our patients showed any visual field loss within the central 12° on the perimetry test.

Figure 4 shows how a model of healthy motion processing (green curve) is affected by simulating increased RGC noise inputs (red curve) or by removing half the RGC inputs (blue curve). The healthy model reproduces the behavior of normally sighted observers, and the unhealthy model with nonfunctional RGC inputs reproduces the behavior of patients with glaucoma. In conclusion, the present data confirm that there is motion-sensitivity impairment in glaucoma. Our technique extend these findings, first by identifying the source of the deficit as a loss in efficiency rather than an elevation in noise in motion sensors and second by identifying impairments in retinal locations not yet suffering from deep visual field loss.

Our analysis suggests that there is no elevation in internal RGC noise in POAG, but a that there is a reduction in RGC sampling efficiency. Reduced sampling efficiency could be caused by RGC loss, which has been shown histologically to occur in human[18,23,45,80,81] and experimental[22,45,82–84] glaucoma. It is also possible that efficiency loss could occur if RGCs become insensitive and nonresponsive. In the earlier stages of the disease, RGCs may become noisy before ultimately undergoing apoptosis or necrosis. If this were the case, we might expect to find increased levels of internal noise as well as reduced levels of sampling efficiency in a group of patients with POAG in the earlier stages of disease. However, our patients with relatively advanced POAG showed no evidence of elevated RGC noise.

## Motion-Sensitivity Loss across the Retina

We found that, although there was no significant change in internal noise across the visual field (there was a small but nonsignificant increase in internal noise with eccentricity), there was a significant drop in sampling efficiency with eccentricity in the healthy young and the old observers. This finding is consistent with the fall-off in RGC density in the peripheral visual field,[81,85] without any increase in RGC noise or increased levels of preretinal light scatter from the ocular media. Our results are in agreement with Atchley and Anderson,[86] who found that motion-coherence detection thresholds for optic flow stimuli increased up to 20° of eccentricity, after which there was no further threshold increase. However, they failed to show an age effect with their radial optic flow stimuli, possibly because of the limitations of high-contrast random dot stimuli described earlier. Similar results have been found for other visual tasks such as face recognition.[77] Makela et al.[77] used a signal-to-noise, contrast-discrimination task analogous to the motion task used in our experiment. They found that contrast thresholds increase in the periphery due to inefficient sampling, not to higher internal noise levels.

## Motion-Sensitivity Loss with Age

Our results show that there is a significant reduction in motion-discrimination thresholds for complex natural optic-flow stimuli in normal ageing. This finding is in agreement with other psychophysical studies showing reduced motion sensitivity with age using random dots[33,53–56,87] or gratings.[57–59] Generally, older observers have elevated motion thresholds (e.g., motion coherence, direction and speed, detection and discrimination), depending on the level of contrast, speed and type of stimuli. There is agreement that this reduction cannot be ex-

plained by optical factors (e.g., neural noise, increased light scatter by lens opacities or senile miosis) alone, and that neural degeneration in the visual system[55–57,59,88] is an important factor in motion-sensitivity loss. Our results provide new insight into the origin of this sensitivity loss. The EN paradigm is able to separate noise and sampling factors, and our results show that the impaired motion sensitivity is due to both a reduction in sampling efficiency and an increase in internal noise with age. The decreased sampling efficiency can be explained by age-related RGC loss across the retina.[23,89] It is also possible that neural degeneration higher up in the visual system[90–92] plays a role, as well. The increase in internal noise with age is in line with sensitivity loss due to increased RGC noise and/or increased light scatter by lens opacities or senile miosis.[93,94] The finding that internal noise does not change with eccentricity indicates that whether it is caused by RGC noise and/or optical factors, it is constant across retinal eccentricity.

## Summary and Conclusions

We confirm that sensitivity to moving stimuli decreases with age and eccentricity and is further impaired in patients with POAG. Functionally, this impairment has implications for locomotion, navigation, and judging time to collision with another stationary or moving object and is important for patients with POAG who experience mobility and navigation problems and in normal aging for everyday visual motion-based tasks such as driving.

For the first time in living observers, our EN analysis and a model with RGC lesions suggest that the motion-sensitivity impairment in advanced glaucoma is almost entirely attributable to a reduction in sampling efficiency with little evidence of the presence of noisy RGCs.

## *References*


1. Resnikoff S, Pascolini D, Etya'ale D, Pararajasegaram R, Pokharel GP, Mariotti SP. Global data on visual impairment in the year 2002. *Bull World Health Organ.* 2004;82:844–851.
2. Saw SM, Foster PJ, Gazzard G, Seah S. Causes of blindness, low vision, and questionnaire-assessed poor visual function in Singaporean Chinese adults: The Tanjong Pagar Survey. *Ophthalmology.* 2004;111:1161–1168.
3. Kingman S. Glaucoma is second leading cause of blindness globally. *Bull World Health Organ*. 2004;82:887–888.
4. Tuck MW, Crick RP. The age distribution of primary open angle glaucoma. *Ophthalmic Epidemiol.* 1998;5:173–183.
5. Anton A, Andrada MT, Mujica V, Calle MA, Portela J, Mayo A. Prevalence of primary open-angle glaucoma in a Spanish population: the Segovia study. *J Glaucoma.* 2004;13:371–376.
6. Iwase A, Suzuki Y, Araie M, et al. The prevalence of primary open-angle glaucoma in Japanese: the Tajimi Study. *Ophthalmology.* 2004;111:1641–1648.
7. Mitchell P, Lee AJ, Rochtchina E, Wang JJ. Open-angle glaucoma and systemic hypertension: the Blue Mountains Eye Study. *J Glaucoma*. 2004;13:319–326.
8. Varma R, Ying-Lai M, Francis BA, et al. Prevalence of open-angle glaucoma and ocular hypertension in Latinos: the Los Angeles Latino Eye Study. *Ophthalmology*. 2004;111:1439–1448.
9. Ntim-Amponsah CT, Amoaku WM, Ofosu-Amaah S, et al. Prevalence of glaucoma in an African population. *Eye* 2004;18:491–497.
10. Quigley HA, Vitale S. Models of open-angle glaucoma prevalence and incidence in the United States. *Invest Ophthalmol Vis Sci.* 1997;38:83–91.
11. Taylor HR, Keeffe JE. World blindness: a 21st century perspective. *Br J Ophthalmol*. 2001;85:261–266.
12. Osborne NN, Wood JP, Chidlow G, Bae JH, Melena J, Nash MS. Ganglion cell death in glaucoma: what do we really know? *Br J Ophthalmol*. 1999;83:980–986.
13. Gupta N, Ang LC, Noel de Tilly L, Bidaisee L, Yucel YH. Human glaucoma and neural degeneration in intracranial optic nerve, lateral geniculate nucleus, and visual cortex. *Br J Ophthalmol*. 2006;90:674–678.
14. Weinreb RN, Khaw PT. Primary open-angle glaucoma. *Lancet*. 2004;363:1711–1720.
15. Wild JM. Techniques and developments in automated perimetry: a review. *Ophthalmic Physiol Opt.* 1988;8:295–308.
16. Anderson AJ, Johnson CA, Fingeret M, et al. Characteristics of the normative database for the Humphrey matrix perimeter. *Invest Ophthalmol Vis Sci*. 2005;46:1540–1548.
17. Anderson RS. The psychophysics of glaucoma: improving the structure/function relationship. *Prog Retin Eye Res.* 2006;25:79–97.
18. Quigley HA, Dunkelberger GR, Green WR. Retinal ganglion cell atrophy correlated with automated perimetry in human eyes with glaucoma. *Am J Ophthalmol.* 1989;107:453–464.
19. Quigley HA, Katz J, Derick RJ, Gilbert D, Sommer A. An evaluation of optic disc and nerve fiber layer examinations in monitoring progression of early glaucoma damage. *Ophthalmology*. 1992;99:19–28.
20. Johnson CA, Sample PA, Cioffi GA, Liebmann JR, Weinreb RN. Structure and function evaluation (SAFE): II. Comparison of optic disk and visual field characteristics. *Am J Ophthalmol.* 2003;135:148–154.
21. Quigley HA, Addicks EM, Green WR. Optic nerve damage in human glaucoma. III. Quantitative correlation of nerve fiber loss and visual field defect in glaucoma, ischemic neuropathy, papilledema, and toxic neuropathy. *Arch Ophthalmol.* 1982;100:135–146.
22. Harwerth RS, Carter-Dawson L, Shen F, Smith EL 3rd, Crawford ML. Ganglion cell losses underlying visual field defects from experimental glaucoma. *Invest Ophthalmol Vis Sci.* 1999;40:2242–2250.
23. Kerrigan-Baumrind LA, Quigley HA, Pease ME, Kerrigan DF, Mitchell RS. Number of ganglion cells in glaucoma eyes compared with threshold visual field tests in the same persons. *Invest Ophthalmol Vis Sci*. 2000;41:741–748.
24. Garway-Heath DF, Holder GE, Fitzke FW, Hitchings RA. Relationship between electrophysiological, psychophysical, and anatomical measurements in glaucoma. *Invest Ophthalmol Vis Sci.* 2002;43:2213–2220.
25. Sommer A, Katz J, Quigley HA, et al. Clinically detectable nerve fiber atrophy precedes the onset of glaucomatous field loss. *Arch Ophthalmol.* 1991;109:77–83.
26. Artes PH, Chauhan BC. Longitudinal changes in the visual field and optic disc in glaucoma. *Prog Retin Eye Res.* 2005;24:333–354.
27. Lachenmayr BJ, Drance SM, Chauhan BC, House PH, Lalani S. Diffuse and localized glaucomatous field loss in light-sense, flicker and resolution perimetry. *Graefes Arch Clin Exp Ophthalmol.* 1991;229:267–273.
28. Spry PG, Johnson CA, Mansberger SL, Cioffi GA. Psychophysical investigation of ganglion cell loss in early glaucoma. *J Glaucoma.* 2005;14:11–19.
29. Johnson CA, Samuels SJ. Screening for glaucomatous visual field loss with frequency-doubling perimetry. *Invest Ophthalmol Vis Sci.* 1997;38:413–425.
30. Baez KA, McNaught AI, Dowler JG, Poinoosawmy D, Fitzke FW, Hitchings RA. Motion detection threshold and field progression in normal tension glaucoma. *Br J Ophthalmol.* 1995;79:125–128.
31. Westcott MC, Fitzke FW, Hitchings RA. Abnormal motion displacement thresholds are associated with fine scale luminance sensitivity loss in glaucoma. *Vision Res.* 1998;38:3171–3180.
32. Bullimore MA, Wood JM, Swenson K. Motion perception in glaucoma. *Invest Ophthalmol Vis Sci.* 1993;34:3526–3533.
33. Trick GL, Steinman SB, Amyot M. Motion perception deficits in glaucomatous optic neuropathy. *Vision Res.* 1995;35:2225–2233.
34. Joffe KM, Raymond JE, Chrichton A. Motion coherence perimetry in glaucoma and suspected glaucoma. *Vision Res.* 1997;37:955–964.
35. Bosworth CF, Sample PA Gupta N, Bathija R, Weinreb RN. Motion automated perimetry identifies early glaucomatous field defects. *Arch Ophthalmol.* 1998;116:1153–1158.

36. Anderson RS, O'Brien C. Psychophysical evidence for a selective loss of M ganglion cells in glaucoma. *Vision Res.* 1997;37:1079–1083.
37. McKendrick AM, Badcock DR, Morgan WH. The detection of both global motion and global form is disrupted in glaucoma. *Invest Ophthalmol Vis Sci.* 2005:46;3693–3701.
38. Sample PA, Boynton RM, Weinreb RN. Isolating the color vision loss in primary open-angle glaucoma. *Am J Ophthalmol.* 1988;106:686–691.
39. Sample PA, Weinreb RN. Progressive color visual field loss in glaucoma. *Invest Ophthalmol Vis Sci.* 1992;33:2068–2071.
40. Sample PA, Weinreb RN. Color perimetry for assessment of primary open-angle glaucoma. *Invest Ophthalmol Vis Sci.* 1990;31:1869–1875.
41. Casson EJ, Johnson CA, Shapiro LR. Longitudinal comparison of temporal-modulation perimetry with white-on-white and blue-on-yellow perimetry in ocular hypertension and early glaucoma. *J Opt Soc Am A Opt Image Sci Vis.* 1993;10:1792–1806.
42. Johnson CA, Adams AJ, Casson EJ, Brandt JD. Blue-on-yellow perimetry can predict the development of glaucomatous visual field loss. *Arch Ophthalmol.* 1993;111:645–650.
43. Hicks TP, Lee BB, Vidyasagar TR. The responses of cells in macaque lateral geniculate nucleus to sinusoidal gratings. *J Physiol.* 1983;337:183–200.
44. Derrington AM, Lennie P. Spatial and temporal contrast sensitivities of neurones in lateral geniculate nucleus of macaque. *J Physiol.* 1984;357:219–240.
45. Quigley HA, Sanchez RM, Dunkelberger GR, L'Hernault NL, Baginski T. A. Chronic glaucoma selectively damages large optic nerve fibers. *Invest Ophthalmol Vis Sci.* 1987;28:913–920.
46. Sample PA, Bosworth CF, Blumenthal EZ, Girkin C, Weinreb RN. Visual function-specific perimetry for indirect comparison of different ganglion cell populations in glaucoma. *Invest Ophthalmol Vis Sci.* 2000;41:1783–1790.
47. Graham SL, Drance SM, Chauhan BC, et al. Comparison of psychophysical and electrophysiological testing in early glaucoma. *Invest Ophthalmol Vis Sci.* 1996;37:2651–2662.
48. Swindale NV, Fendick MG, Drance SM, Graham SL, Hnik P. Contrast sensitivity for flickering and static letters and visual acuity at isoluminance in glaucoma. *J Glaucoma.* 1996;5:156–169.
49. McKendrick AM, Badcock DR, Morgan WH. Psychophysical measurement of neural adaptation abnormalities in magnocellular and parvocellular pathways in glaucoma. *Invest Ophthalmol Vis Sci.* 2004;45:1846–1853.
50. Ansari EA, Morgan JE, Snowden RJ. Psychophysical characterisation of early functional loss in glaucoma and ocular hypertension. *Br J Ophthalmol.* 2002;86:1131–1135.
51. Ansari EA, Morgan JE, Snowden RJ. Glaucoma: squaring the psychophysics and neurobiology. *Br J Ophthalmol.* 2002;86:823–826.
52. Merigan WH, Maunsell JH. How parallel are the primate visual pathways? *Annu Rev Neurosci.* 1993;16:369–402.
53. Atchley P, Andersen GJ. The effect of age, retinal eccentricity, and speed on the detection of optic flow components. *Psychol Aging.* 1998;13:297–308.
54. Gilmore GC, Wenk HE, Naylor LA, Stuve TA. Motion perception and aging. *Psychol Aging.* 1992;7:654–660.
55. Tran DB, Silverman SE, Zimmerman K, Feldon SE. Age-related deterioration of motion perception and detection. *Graefes Arch Clin Exp Ophthalmol.* 1998;236:269–273.
56. Trick GL, Silverman SE. Visual sensitivity to motion: age-related changes and deficits in senile dementia of the Alzheimer type. *Neurology.* 1991;41:1437–1440.
57. Willis A, Anderson SJ. Effects of glaucoma and aging on photopic and scotopic motion perception. *Invest Ophthalmol Vis Sci.* 2000;41:325–335.
58. Betts LR, Taylor CP, Sekuler AB, Bennett PJ. Aging reduces center-surround antagonism in visual motion processing. *Neuron.* 2005;45:361–366.
59. Snowden RJ, Kavanagh E. Motion perception in the ageing visual system: minimum motion, motion coherence, and speed discrimination thresholds. *Perception.* 2006;35:9–24.
60. Turano KA, Rubin GS, Quigley HA. Mobility performance in glaucoma. *Invest Ophthalmol Vis Sci.* 1999;40:2803–2809.
61. Turano KA, Yu D, Hao L, Hicks JC. Optic-flow and egocentric-direction strategies in walking: central vs peripheral visual field. *Vision Res.* 2005;45:3117–3132.
62. Lovie-Kitchin JE, Mainstone J, Robinson J, Brown B. What areas of the visual field are important for mobility in low vision patients? *Clin Vis Sci.* 1990;5:249–263.
63. The Advanced Glaucoma Intervention Study (AGIS): 9. Comparison of glaucoma outcomes in black and white patients within treatment groups. *Am J Ophthalmol.* 2001;132:311–320.
64. Bex PJ, Dakin SC, Mareschal I. Critical band masking in optic flow. *Network* .2005;16:261–284.
65. Tyler CW. Colour bit-stealing to enhance the luminance resolution of digital displays on a single pixel basis. *Spat Vis.* 1997;10:369–377.
66. Brainard DH. The Psychophysics Toolbox. *Spat Vis.* 1997;10:433–436.
67. Wetherill GB, Levitt H. Sequential estimation of points on a psychometric function. *Br J Math Stat Psychol.* 1965;18:1–10.
68. Barlow HB. Retinal noise and absolute threshold. *J Opt Soc Am.* 1956;46:634–639.
69. Watt RJ, Morgan MJ. Spatial filters and the localization of luminance changes in human vision. *Vision Res.* 1984;24:1387–1397.
70. Dakin SC. Information limit on the spatial integration of local orientation signals. *J Opt Soc Am A Opt Image Sci Vis.* 2001;18:1016–1026.
71. Simpson WA, Falkenberg HK, Manahilov V. Sampling efficiency and internal noise for motion detection, discrimination, and summation. *Vision Res.* 2003;43:2125–2132.
72. Dakin SC, Mareschal I, Bex PJ. Local and global limitations on direction integration assessed using equivalent noise analysis. *Vision Res.* 2005;45:3027–3049.
73. Green DM. *Signal Detection Theory and Psychophysics.* New York: John Wiley & Sons; 1966.
74. Foster DH, Bischof WF. Bootstrap variance estimators for the parameters of small-sample sensory-performance functions. *Biol Cybern.* 1987;57:341–347.
75. Faraway JJ. *Linear Models with R.* Boca Raton, FL: Chapman & Hall/CRC; 2004.
76. Eckstein MP, Whiting JS, Thomas JP. Detection and contrast discrimination of moving signals in uncorrelated Gaussian noise. *SPIE Proc.* 1996;2712:9–25.
77. Makela P, Nasanen R, Rovamo J, Melmoth D. Identification of facial images in peripheral vision. *Vision Res.* 2001;41:599–610.
78. Adelson EH, Bergen JR. Spatiotemporal energy models for the perception of motion. *J Opt Soc Am A.* 1985;2:284–299.
79. Fine I, Anderson CM, Boynton GM, Dobkins KR. The invariance of directional tuning with contrast and coherence. *Vision Res.* 2004;44:903–913.
80. Mikelberg FS, Yidegiligne HM, Schulzer M. Optic nerve axon count and axon diameter in patients with ocular hypertension and normal visual fields. *Ophthalmology.* 1995;102:342–348.
81. Harwerth RS, Carter-Dawson L, Smith EL 3rd, Barnes G, Holt WF, Crawford ML. Neural losses correlated with visual losses in clinical perimetry. *Invest Ophthalmol Vis Sci.* 2004;45:3152–3160.
82. Glovinsky Y, Quigley HA, Pease ME. Foveal ganglion cell loss is size dependent in experimental glaucoma. *Invest Ophthalmol Vis Sci.* 1993;34:395–400.
83. Glovinsky Y, Quigley HA, Dunkelberger GR. Retinal ganglion cell loss is size dependent in experimental glaucoma. *Invest Ophthalmol Vis Sci.* 1991;32:484–491.
84. Quigley HA, Addicks EM. Chronic experimental glaucoma in primates. II. Effect of extended intraocular pressure elevation on optic nerve head and axonal transport. *Invest Ophthalmol Vis Sci.* 1980;19:137–152.
85. Curcio CA, Allen KA. Topography of ganglion cells in human retina. *J Comp Neurol.* 1990;300:5–25.
86. Atchley P, Andersen GJ. The discrimination of heading from optic flow is not retinally invariant. *Percept Psychophys.* 1999;61:387–396.

87. Norman JF, Clayton AM, Shular CF, Thompson SR. Aging and the perception of depth and 3-D shape from motion parallax. *Psychol Aging.* 2004;19:506–514.
88. Elliott D, Whitaker D, MacVeigh D. Neural contribution to spatiotemporal contrast sensitivity decline in healthy ageing eyes. *Vision Res.* 1990;30: 541–547.
89. Harman A, Abrahams B, Moore S, Hoskins R. Neuronal density in the human retinal ganglion cell layer from 16–77 years. *Anat Rec.* 2000;260:124–131.
90. Devaney KO, Johnson HA. Neuron loss in the aging visual cortex of man. *J Gerontol.* 1980;35:836–841.
91. Marner L, Nyengaard JR, Tang Y, Pakkenberg B. Marked loss of myelinated nerve fibers in the human brain with age. *J Comp Neurol.* 2003;462:144–152.
92. Pakkenberg B, Pelvig D, Marner L, et al. Aging and the human neocortex. *Exp Gerontol.* 2003;38:95–99.
93. Johnson CA, Adams AJ, Lewis RA. Evidence for a neural basis of age-related visual field loss in normal observers. *Invest Ophthalmol Vis Sci.* 1989;30:2056–2064.
94. Pardhan S. Contrast sensitivity loss with aging: sampling efficiency and equivalent noise at different spatial frequencies. *J Opt Soc Am A Opt Image Sci Vis.* 2004;21:169–175.